Probing composite Higgs boson substructure at the HL-LHC

Probing composite Higgs boson substructure at the HL-LHC

Avik Banerjee,[1,2,*] Sayan Dasgupta,[3,†] and Tirtha Sankar Ray[3,‡]

[1]*Department of Physics, Chalmers University of Technology, Fysikgården, 41296 Göteborg, Sweden*
[2]*Saha Institute of Nuclear Physics, HBNI, 1/AF Bidhan Nagar, Kolkata 700064, India*
[3]*Department of Physics, Indian Institute of Technology Kharagpur, Kharagpur 721302, India*

(Received 16 August 2021; accepted 28 October 2021; published 29 November 2021)

The Higgs boson may well be a composite scalar with a finite extension in space. Owing to the momentum dependence of its couplings, the imprints of such a composite pseudo Goldstone Higgs may show up in the tails of various kinematic distributions at the LHC, distinguishing it from an elementary state. From the bottom up, we construct the momentum-dependent form factors to capture the interactions of the composite Higgs with the weak gauge bosons. We demonstrate their impact in the differential distributions of various kinematic parameters for the $pp \to Z^*H \to l^+l^-b\bar{b}$ channel. We show that this channel can provide an important handle to probe the Higgs' substructure at the HL-LHC.

DOI: 10.1103/PhysRevD.104.095021

I. INTRODUCTION

Since its discovery [1,2], the properties of the Higgs particle have been under intense theoretical and experimental scrutiny. A primary question relates to the existence of possible internal structure of the Higgs boson. The upcoming runs of the Large Hadron Collider (LHC) and all future collider experiments are mandated to study the properties of the Higgs, including exploring the possibility of the Higgs having a finite extension in space.

Interestingly, a composite Higgs having a nontrivial internal structure is known to be a handle in addressing the notorious gauge hierarchy problem of the Standard Model (SM) [3–10]. In this paper, we consider the well-motivated composite Higgs framework where the Higgs is identified with a pseudo Nambu-Goldstone boson (pNGB) of a strongly interacting sector. Within this paradigm, the Higgs boson may be considered as a composite of underlying chiral fermions [11–13]. The compositeness scale Λ_H is related to the length scale $l_H \sim 1/\Lambda_H$ governing the geometric size of the Higgs. To conform with the electroweak precision data, a separation of Λ_H and the weak scale ($v \ll \Lambda_H$) is introduced by considering the Higgs as a pNGB of the strong sector. In this framework, existence of new resonances near the compositeness scale ($m_Q \sim \Lambda_H$) is expected, which can be searched directly at the LHC [14–23]. These exotic states, along with the modification of Higgs couplings, are the two major conventional signatures of this setup that have been actively chased in collider experiments [24–31]. The modifications of the Higgs couplings originate from two sources. First, a deviation from the SM value of the coupling arises due to the nonlinear structure of the pNGB chiral Lagrangian. The measurements of the Higgs signal strengths at the LHC constrain these deviations to less than 10%–15% from their SM values [24–28]. An additional source of modification arises from the extension of the Higgs in space, resulting in a dramatic scaling of the Higgs coupling with the transferred momentum. It is this latter phenomenon that provides a more direct evidence of the nonelementary nature of the Higgs [32–40].

We construct the Higgs-elementary coupling form factors from the bottom up, relying on the empirical Lorentz structure and inspiration from large N tools for composite states [41–43], assuming an underlying strongly interacting hypercolor dynamics. We demonstrate that the high luminosity LHC (HL-LHC) [44] can explore a significant portion of the parameter space where the momentum dependence of the Higgs coupling implies pronounced deviation from the SM predictions in the differential distribution of kinematic parameters. This provides an interesting handle to explore the Higgs compositeness, even if the compositeness scale lies just beyond the LHC reach. As a proof of principle, we consider the $pp \to Z^*H \to l^+l^-b\bar{b}$ channel at the HL-LHC and demonstrate that there is a considerable deviation in the kinematic distributions of the final state objects for this channel that can be used to explore the nonelementary nature of the Higgs boson.

The rest of the paper is organized as follows. In Sec. II, we construct the form factors associated to the Higgs couplings

*avik@chalmers.se
†sayandg05@gmail.com
‡tirthasankar.ray@gmail.com

with the weak gauge bosons. In Sec. III, we perform the collider analysis to demonstrate the importance of the differential distributions in probing the composite nature of the Higgs boson. In this regard, we show the prospects of the HL-LHC in Sec. IV, before concluding in Sec. V.

II. COMPOSITE HIGGS COUPLINGS

In the SM, the Higgs couplings to the massive gauge bosons ($V = W^{\pm}, Z$) are given by

$$\mathcal{L}_{hVV} = g_V^{\rm SM} h V_\mu V^\mu, \quad \text{where } \{g_W^{\rm SM}, g_Z^{\rm SM}\} = \left\{\frac{g^2 v}{2}, \frac{g^2 v}{2\cos^2\theta_W}\right\}, \quad \text{and} \quad v = 246 \text{ GeV}. \tag{2.1}$$

On the other hand, in composite Higgs frameworks, the above coupling can, in general, be written as

$$\mathcal{L}_{hVV} = g_V^{\rm SM} \frac{\Pi_V^{\mu\nu}(p_1, p_2)}{f^2} h V_\mu(p_1) V_\nu(p_2), \tag{2.2}$$

where the scale f denotes the decay constant of the pNGB Higgs. The compositeness scale Λ_H is related to f as $\Lambda_H \sim g_* f$, where g_* represents a generic strong sector coupling as $1 \ll g_* < 4\pi$. The momentum-dependent form factor $\Pi_V^{\mu\nu}$ captures the nonperturbative dynamics of the strong sector leading to a nonelementary Higgs with a finite shape. Assuming the Higgs to be a purely CP-even state, the Lorentz structure of the form factor can be decomposed as [35,45,46]

$$\Pi_V^{\mu\nu} = \left[\Pi_1^V \eta^{\mu\nu} + \frac{1}{\Lambda_H^2}\{\Pi_2^V(\eta^{\mu\nu} p_1.p_2 - p_2^\mu p_1^\nu) + \Pi_3^V p_1^\mu p_2^\nu + \Pi_4^V p_1^\mu p_1^\nu + \Pi_5^V p_2^\mu p_2^\nu\}\right]. \tag{2.3}$$

In the above equation, the momentum-dependent functions $\Pi_i^V(p_1, p_2)$ have mass dimension 2, and we have extracted appropriate powers of Λ_H on the basis of dimensional analysis. Demanding that the SM coupling is reproduced at the low energy ($p_i.p_j \ll \Lambda_H^2$), *modulo* a suppression due to the nonlinearity of the pNGB, we can constrain the IR behavior of $\Pi_V^{\mu\nu}$ as

$$\lim_{p_i.p_j \ll \Lambda_H^2} g_V^{\rm SM} \frac{\Pi_V^{\mu\nu}(p_1, p_2)}{f^2} \simeq g_V^{\rm SM} \frac{\Pi_1^V(0,0)}{f^2} \eta^{\mu\nu} = g_V^{\rm SM} \sqrt{1-\xi}\, \eta^{\mu\nu}. \tag{2.4}$$

The usual suppression by a factor of $\sqrt{1-\xi}$ (where $\xi \equiv v^2/f^2$) is considered to reproduce the hVV coupling in the minimal composite Higgs model. A full nonperturbative calculation is, in general, required to find the detailed momentum dependence of the form factors. However, one can guess some ansatz for Π_i^V from the wisdom of large N formalism [6,7,47–49]. We follow this approach below to adopt an ansatz for the three-point vertex form factors.

A. Large N implications

To progress further, we assume that the strong sector has an underlying confining SU(N) gauge dynamics with a suitably large N. In the large N limit, the n-point correlators between composite operators $\mathcal{O}_1, \mathcal{O}_2, \ldots \mathcal{O}_n$ of this confining theory scales as $\langle \mathcal{O}_1 \mathcal{O}_2 \ldots \mathcal{O}_n \rangle \sim N$ at the leading order [41–43]. In this limit, one can show that a two-point correlation function as shown in Fig. 1(a) can be approximated at the leading order in N as

$$\langle \mathcal{O}(p)\mathcal{O}(-p)\rangle \sim \sum_{a=1}^{\infty} \frac{F_a^2}{p^2 - m_a^2 + i{\rm Im}[M_a^2(p)]}, \quad F_a \equiv \langle 0|\mathcal{O}|a\rangle. \tag{2.5}$$

The masses of the single-particle mesonic states are given as $m_a \equiv g_a F_a$, where $g_a \sim 1/\sqrt{N}$. The large N counting shows that the decay constant $F_a \sim \sqrt{N}$ so that $\langle \mathcal{O}\mathcal{O}\rangle \sim N$. Here, $M_a^2(p)$ represents the radiative corrections to the 1PI resummed propagators of the mesonic states. Similar arguments can be extended to three-point correlators as well, where two different structures are possible as follows [43] [see Figs. 1(b) and 1(c)]:

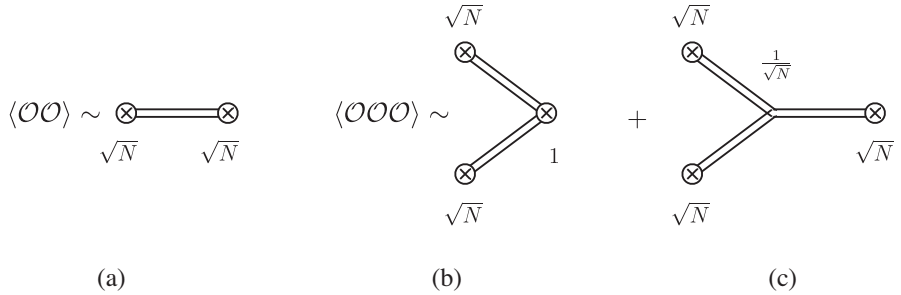

(a) (b) (c)

FIG. 1. Large N scaling for two-point (left) and three-point (right) correlators in a strongly coupled SU(N) gauge theory.

$$\langle \mathcal{O}(p_1)\mathcal{O}(p_2)\mathcal{O}(-p_1-p_2)\rangle \sim \sum_{a,b=1}^{\infty} \frac{F_a F_b \langle 0|\mathcal{O}|ab\rangle}{(p_1^2 - m_a^2 + i\mathrm{Im}[M_a^2(p)])(p_2^2 - m_b^2 + i\mathrm{Im}[M_b^2(p)])}, \tag{2.6}$$

and

$$\langle \mathcal{O}(p_1)\mathcal{O}(p_2)\mathcal{O}(-p_1-p_2)\rangle \sim \sum_{a,b,c=1}^{\infty} \frac{F_a F_b F_c \Gamma_{c\to ab}}{(p_1^2 - m_a^2 + i\mathrm{Im}[M_a^2(p)])(p_2^2 - m_b^2 + i\mathrm{Im}[M_b^2(p)])((p_1+p_2)^2 - m_c^2 + i\mathrm{Im}[M_c^2(p)])}. \tag{2.7}$$

In the first case, one of the operators creates two meson states (with amplitude $\langle 0|\mathcal{O}|ab\rangle$), which are annihilated by the other two operators, while in the second case, each operator excites a single meson, and they interact via a local three-point vertex (given by $\Gamma_{c\to ab}$). Clearly, the leading N scaling suggests that $\langle 0|\mathcal{O}|ab\rangle \sim 1$ and $\Gamma_{c\to ab} \sim 1/\sqrt{N}$.

We apply these results to the composite pNGB Higgs scenario. The relevant correlation function for the hVV coupling is a correlator between three currents $\langle J_\mu J_\nu J_\pi\rangle$. The vector currents $J_{\mu,\nu}$ mix with the weak elementary gauge bosons, implying a linear mixing between the $W^\pm$ and Z bosons with composite spin-1 mesons. The current J_π can excite a pNGB Higgs boson, which is a purely composite condensate. In Fig. 1(b), the Higgs boson is generated from the vacuum by nonperturbative dynamics with a strength proportional to $\langle 0|J_\pi|ab\rangle$, where a, b denotes the two spin-1 meson states. On the other hand, in Fig. 1(c), the pNGB Higgs, which is denoted by the horizontal double line, interacts with the composite mesons through derivative couplings. As a result, the coupling strength $\Gamma_{c\to ab}$ in Eq. (2.7) has an additional $\mathcal{O}(p_h^2/\Lambda_H^2)$ suppression in comparison to Eq. (2.6), where p_h denotes the momentum passing through the Higgs.[1] It is expected that the underlying strong dynamics leads to a unique meson spectrum. As a consequence, all the form factors Π_i^V should have an identical pole structure in the large N limit. Equipped with these results, we adopt an ansatz for Π_i^V at the leading order in N as well as in the momentum passing through the Higgs as

$$\Pi_i(p_1,p_2) = \sum_{a,b=1}^{\infty} \frac{c_i^V F_a F_b \langle 0|J_\pi|ab\rangle}{(p_1^2 - m_a^2 + i\mathrm{Im}[M_a^2(p)])(p_2^2 - m_b^2 + i\mathrm{Im}[M_b^2(p)])}. \tag{2.8}$$

The constant coefficients c_i^V parametrizes our ignorance about the details of the strong dynamics. Although the form factor contains an infinite sum over the meson states, the convergence of the series is ensured by assuming that the masses of the mesonic states appearing in the successive terms are hierarchical [6,7,47–49]. We take the dominant contribution coming from the first term in the summation and use the low energy constraint given in Eq. (2.4) to obtain

$$\Pi_V^{\mu\nu} = \frac{f^2 m_1^2 m_2^2 (1 - i\frac{\Gamma_1}{m_1})(1 - i\frac{\Gamma_2}{m_2})}{(p_1^2 - m_1^2 + i m_1\Gamma_1)(p_2^2 - m_2^2 + i m_2\Gamma_2)} \Big[\sqrt{1-\xi}\eta^{\mu\nu} + \frac{1}{m_1 m_2}\{c_2^V(\eta^{\mu\nu} p_1.p_2 - p_2^\mu p_1^\nu) + c_3^V p_1^\mu p_2^\nu + c_4^V p_1^\mu p_1^\nu + c_5^V p_2^\mu p_2^\nu\}\Big]. \tag{2.9}$$

In the above equation, we use the narrow width approximation to replace $\mathrm{Im}[M_a^2(p)]$ by $m_a\Gamma_a$, where Γ_a denotes the total width of the mesonic states, and identified $\Lambda_H \equiv \sqrt{m_1 m_2}$. Interestingly, the insertion of two lightest meson states in the form factor as above provides a handle to arrive at a convergent radiative Coleman-Weinberg potential for the pNGB Higgs [7,47,48].

The strongly interacting light Higgs (SILH) description provides an alternative way to describe the composite Higgs models through an effective field theory framework [53–61]. The relevant custodial hVV operators at leading order are given by

[1] Another possibility, not considered in this paper, may arise if an elementary Higgs boson mixes with a composite scalar [50–52]. In that case, $\Gamma_{c\to ab}$ denotes local interaction between the additional composite scalar with two spin-1 mesons, which may arise at the same order as Eq. (2.6).

$$\mathcal{L}_{\rm SILH} \supset \frac{c_H}{2f^2}\partial^\mu(H^\dagger H)\partial_\mu(H^\dagger H) + \frac{ic_W g}{2m_\rho^2}(H^\dagger\sigma^a \overleftrightarrow{D^\mu} H)D^\nu W^a_{\mu\nu} + \frac{ic_B g'}{2m_\rho^2}(H^\dagger \overleftrightarrow{D^\mu} H)\partial^\nu B_{\mu\nu}$$
$$+ \frac{ic_{HW} g}{16\pi^2 f^2}(D^\mu H^\dagger)\sigma^a(D^\nu H)W^a_{\mu\nu} + \frac{ic_{HB} g'}{16\pi^2 f^2}(D^\mu H^\dagger)(D^\nu H)B_{\mu\nu}. \tag{2.10}$$

If we identify $m_1 = m_2 = m_\rho \lesssim 4\pi f$, then the effective hVV coupling obtained from the SILH Lagrangian can be mapped into the leading order expansion $\sim\mathcal{O}(p^2/m_\rho^2)$ of the form factor, as shown in Appendix.

We take a quick look at the existing constraints on the hVV couplings to device our benchmark. Modification of the Higgs couplings by measuring inclusive cross sections of the Higgs production processes at the LHC Run 2 exclude $f \leq 1$ TeV [25,26]. Although the constraints from electroweak precision data have considerable dependence on the UV constructions [7,49,62–64], a somewhat conservative limit of $m_{1,2} \gtrsim 2$–3 TeV is reported in [65]. Similarly, a direct search of nonstandard vector bosons at the LHC puts a limit on the masses of these exotic states in the same ballpark region [20–23,66], though the individual analyses involve several assumptions on model parameters and branching ratios to specific channels. Considering the values of ξ, allowed by the Higgs coupling measurements, we find that the limits on the $m_{1,2}$ from unitarity [67,68] is considerably weaker than the electroweak precision data and direct search limits. Current limits on the SILH coefficients are extracted from [69–72] and listed in the Appendix. However, using these limits to arbitrarily high momenta ($p^2 \gg M_W^2$) is not justified as it will violate the EFT expansion [46].

III. PROBING THE HIGGS FORM FACTOR AT COLLIDER EXPERIMENTS

In this section, we explore the possibility of utilizing the $pp \to Z^*H \to l^+l^-b\bar{b}$ channel (where $l = e, \mu$, see Fig. 2) to probe the hZZ form factor introduced in Eqs. (2.2) and (2.9). In contrast to the conventional searches for the Higgs-strahlung process at the LHC [73,74], we focus on the tails of the distributions of various kinematic observables where the Z boson is far off shell. Despite a relatively low cross section, it is easier to get an off-shell Z in the associated Higgs production mode in comparison to the weak boson fusion or processes involving decay of Higgs into diboson. In particular, the presence of a s-channel Z boson in the Z^*H production mode proves to be most advantageous to probe the impact of the form factor.

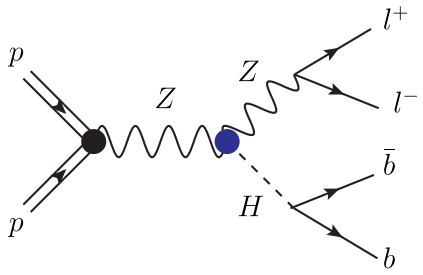

FIG. 2. Feynman diagram corresponding to the $pp \to Z^*H \to l^+l^-b\bar{b}$ process. The form factor involved in the hZZ vertex is denoted by the blue blob.

The form factor is implemented in the SM Universal Feynrules Output (UFO) format in MadGraph5 [75]. Guided by the existing constraints presented in the previous section, we consider $\xi = 0.06$, $m_1 = m_2 = 2.5$ TeV, and $c^Z_{i\neq 1} = 1$ as the benchmark values to present our results. Note that the second term in Eq. (2.3) also receives a contribution from the SM at one loop; however, we have encoded that contribution inside the free parameter c_2^Z together with the effects from the strong dynamics. Composite Higgs models generically predict the existence of broad spin-1 resonances [76,77]. Here, we take a purely phenomenological approach and choose two extreme benchmark cases $\Gamma_{1,2}/m_{1,2} = 1\%$ and 20% to compare the impact of a narrow and a broad resonance in the differential distributions. We assume SM-like Higgs-bottom coupling in our analysis.[2]

The parton level cross section for the Higgs-strahlung process ($q\bar{q} \to ZH$), assuming $m_1 = m_2$ ($\Gamma_1 = \Gamma_2$) and neglecting the light quark masses, is given by

$$\sigma(\hat{s}) = \frac{\sigma^{\rm SM}(\hat{s}) m_1^8 (1+\frac{\Gamma_1^2}{m_1^2})^2}{[(\hat{s}-m_1^2)^2 + m_1^2\Gamma_1^2][(M_Z^2-m_1^2)^2 + m_1^2\Gamma_1^2]}$$
$$\times \left[(1-\xi) - \frac{24\sqrt{1-\xi}c_2^Z M_Z^2\sqrt{\frac{\lambda^2}{4}+\frac{M_Z^2}{\hat{s}}}}{m_1^2(\lambda^2+\frac{12M_Z^2}{\hat{s}})} + \mathcal{O}\left(\frac{v^4}{m_1^4}\right)\right], \tag{3.1}$$

where[3]

[2]Unlike the hVV term, the modification of the Yukawa coupling in partial compositeness framework depends on the details of the model. More specifically, it depends on which representation of the global symmetry of the strong sector is used to embed the bottom quark. To avoid this model specific uncertainties, we assume the $hb\bar{b}$ coupling to be equal to its SM value. As an example, in MCHM$_4$ scenario, modification of the $hb\bar{b}$ coupling leads to a overall reduction of the cross section by 6% (for $f = 1$ TeV).

[3]The coefficients v_q and a_q denote the vector and axial vector couplings of the $q\bar{q}$ pair with the Z boson.

$$\sigma^{\rm SM}(\hat{s}) = \frac{(g_Z^{\rm SM})^2(v_q^2+a_q^2)\lambda\hat{s}(\lambda^2+\frac{12M_Z^2}{\hat{s}})}{576\pi M_Z^2[(\hat{s}-M_Z^2)^2+M_Z^2\Gamma_Z^2]},$$
$$\lambda = \sqrt{\left(1-\frac{M_Z^2}{\hat{s}}-\frac{m_h^2}{\hat{s}}\right)^2-\frac{4M_Z^2m_h^2}{\hat{s}^2}}. \quad (3.2)$$

In the above equation, the terms proportional to c_3^Z, c_4^Z, c_5^Z are neglected in the limit where the quark masses are negligible. In Fig. 3, we display the cross section of the parton level process ($q\bar{q} \to ZH$) as a function of the partonic center of mass energy $\sqrt{\hat{s}}$ for the elementary (red) and the composite Higgs setup with $\Gamma_{1,2}/m_{1,2} = 1\%$ (blue) and $\Gamma_{1,2}/m_{1,2} = 20\%$ (magenta, dashed). The simulated results with our implementation of the form factor given in Eq. (2.9) are also plotted in the same figure and match well with the theoretical prediction for the cross section discussed above. Figure 3 shows that the presence of momentum-dependent couplings at the hZZ vertex in contrast to the elementary Higgs scenario causes an enhancement of the cross section near the tail of the distribution and eventually leads to a peak at $m_{1,2}$ due to the pole structure of Eq. (2.9). However, we expect additional threshold contributions (depending on specific UV completion) near the $\sqrt{\hat{s}} \sim m_{1,2}$ that may significantly modify the cross section in this region. The gray dotted curve in the Fig. 3 denotes the cross section in the effective SILH framework as given in the Eq. (2.10), with $c_H = 1$, $c_W = c_B = 1/2$, and $c_{HW} = c_{HB} = (8\pi^2 f^2/m_1^2) \simeq 12$. The dependence of the cross section on the parameters c_{HW} and c_{HB} are milder than the others. This choice of coefficients is adapted to match with the leading order expansion of our form factor parametrization and is well within the present limits (see Appendix for details). In the region displayed in Fig. 3, the SILH result matches fairly well with that obtained using the form factors when only the leading order terms in the expansion around $\hat{s}/m_1^2$ are kept in Eq. (3.1). However, the cross section at high center of mass energies for the SILH case grows with energy as $\sigma \sim \hat{s}/m_\rho^4$, which would lead to a violation of tree level unitarity [57]. To correct for this, the SILH framework needs to be supplemented with higher derivative terms and additional dynamic degrees of freedom near the threshold region $\hat{s} \gtrsim m_\rho^2$. On the other hand, the cross section using the form factor decreases with $\hat{s}$ at large energies as $\sigma \sim M_Z^2/\hat{s}^2$, thereby preserving unitarity. Thus, for the differential distributions, the form factor defined in Eq. (2.9) may provide a more tractable resume of the composite Higgs in contrast with the elementary case.

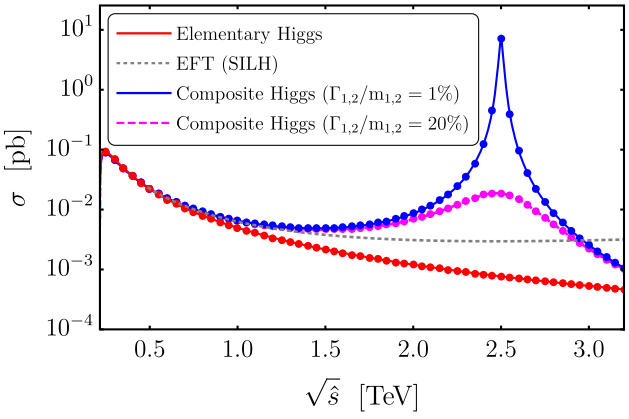

FIG. 3. Variation of cross section given in Eqs. (3.1) and (3.2) with partonic center of mass energy ($\sqrt{\hat{s}}$) for the elementary (red) and the composite Higgs scenario with $\Gamma_{1,2}/m_{1,2} = 1\%$ (blue) and 20% (magenta, dashed) are displayed. For comparison, the cross section for the SILH framework (gray, dotted) is also shown. To validate the implementation of the form factor in MadGraph5, we plot the simulated cross section by different colored points.

In passing, we note that the form factor scenario discussed here can, in principle, be distinguished from the s-channel exchange of a weakly coupled BSM particle like a Z' boson with $hZ'Z'$ coupling. Unlike the case for a Z', the form factor with proper normalization as given in the Eq. (2.9) does not give any propagator suppression away from the pole of the mesonic states; rather, it approaches 1. Further, the interference between the Z' mediated process and the SM process creates differences in the distribution. There is discernible distortion in the line shape around the pole compared to the form factor case, making them easily distinguishable.

We generate 10^5 events at the leading order (LO) and at center of mass energy $\sqrt{s} = 14$ TeV for both the elementary and the composite Higgs scenario in MadGraph5, after applying the generator level cuts listed in Table I. These cuts have been chosen to remove soft b jets and leptons and to ensure that the dilepton pair and the $b\bar{b}$ pair are produced from the final state objects. We parton shower the events using PYTHIA8 [78], jet cluster using FastJet [79], pass them through detector simulation in DELPHES [80] using the default CMS card, and finally generate the distributions in MadAnalysis5 [81].

In Fig. 4, we present the distributions of various kinematic parameters for the elementary (red) and the composite Higgs with $\Gamma_{1,2}/m_{1,2} = 1\%$ (blue) and 20% (magenta, dashed). In the vertical axis, we plot the normalized events $N_i = \mathcal{N}_i/\mathcal{N}_{\rm tot}$, where $\mathcal{N}_i$ and $\mathcal{N}_{\rm tot}$ denote the number of events in the ith bin and the total number of events for each scenario, respectively. We

TABLE I. Generator level cuts on the transverse momenta ($p_T^{l,b}$), pseudorapidity ($\eta_{l,b}$), and the angular separation ($\Delta R_{l^+l^-,b\bar{b}}$) of the final state objects, which are used to remove soft b jets and leptons and to assure that the l^+l^- and the $b\bar{b}$ pairs are produced from same outer legs, respectively.

Observable	$p_T^{l,b}$	$\eta_{l,b}$	$\Delta R_{l^+l^-,b\bar{b}}$
Cut	> 25 GeV	< 2.5	< 3.0

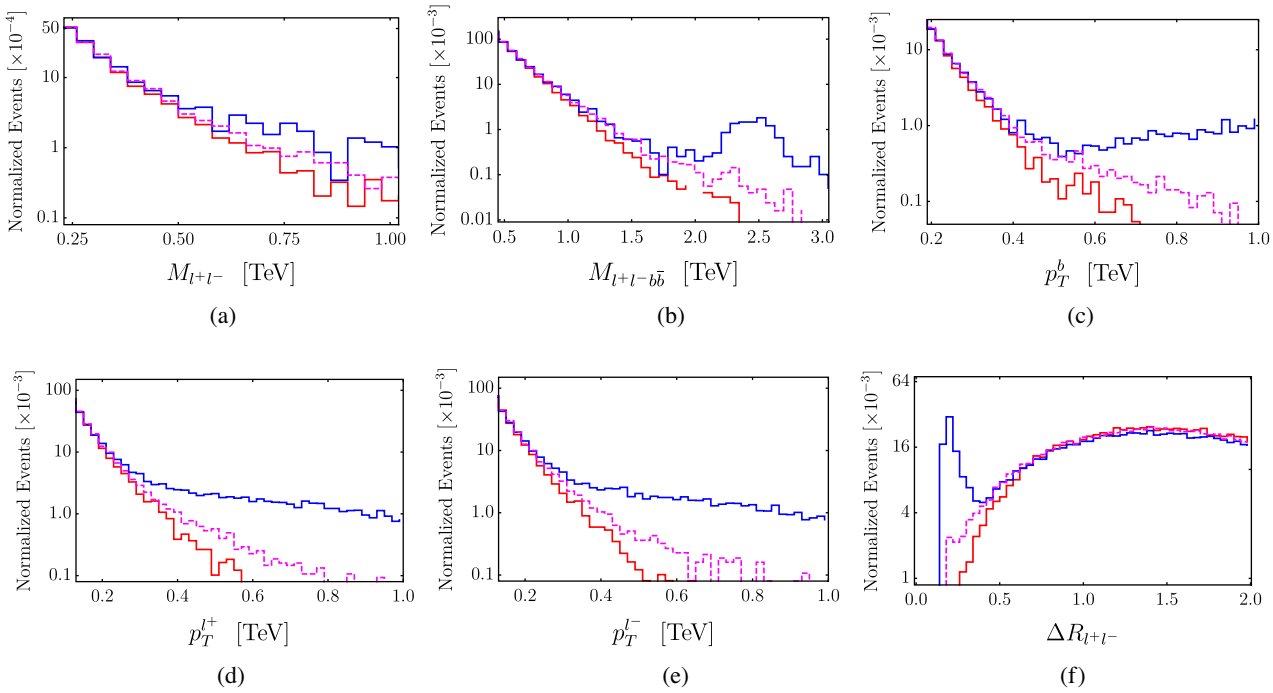

FIG. 4. Reconstructed level event distributions for observables displaying significant enhancement for the composite Higgs scenario with $\Gamma_{1,2}/m_{1,2} = 1\%$ (blue) and 20% (magenta, dashed) over the elementary case (red) near the tails. We choose $\xi = 0.06$, $m_1 = m_2 = 2.5$ TeV, and $c^Z_{i\neq 1} = 1$. The normalized events in the vertical axis represent the number of simulated events normalized to one event.

highlight the tails of the distributions where some deviations from the elementary case can be observed for all the observables presented. Leptons being one of the cleanest final state at the LHC, $p_T^{l^\pm}$ and $\Delta R_{l^+l^-}$ may provide an acceptable signal over the background, as discussed in the next section. The enhancement over the elementary scenario is pronounced when one of the momenta appearing in the form factor comes close to m_1 or m_2. Larger enhancement of the cross section at the tail is observed for the form factor involving narrower composite states. Evidently, with smaller values of $m_{1,2}$, more pronounced effects can be observed. In Fig. 4, the bump for $\Gamma_{1/2}/m_{1/2} = 1\%$ at small values of $\Delta R_{l^+l^-}$ corresponds to highly collimated final state leptons. The bump arises as a consequence of the threshold effects around $s \sim m^2_{1,2}$ due to the unique pole structure of the form factor in Eq. (2.9). The bump is suppressed for $\Gamma_{1/2}/m_{1/2} = 20\%$ due to the diminished cross section around the threshold region for wide resonances. One interesting possibility is to investigate the hadronic decay of the Z boson near the resonance, which has a larger branching ratio than the leptonic channel. The fat jets formed due to the collimation of the hadronic decay products of Z near the pole of the form factor can be employed to efficiently discriminate the signal from the background using the jet substructure techniques [82]. However, we concentrate on

TABLE II. LO cross sections and efficiencies for the signal (keeping $m_1 = m_2 = 2.5$ TeV) and background processes at 14 TeV using our benchmark parameters and after applying the generator level cuts in MadGraph5.

Signal	Cross section (pb)	Efficiency
Composite Higgs ($\Gamma_{1,2}/m_{1,2} = 1\%$)	0.0109 ± 0.0003	1.5×10^{-2}
Composite Higgs ($\Gamma_{1,2}/m_{1,2} = 20\%$)	0.0098 ± 0.0002	1.5×10^{-2}
Elementary Higgs	0.0100 ± 0.0002	1.3×10^{-2}
Background	Cross section (pb)	Efficiency
$t\bar{t}(\to l^+l^- + b\bar{b} + \not{E}_T)$	6.23 ± 0.01	2.0×10^{-5}
$tW(\to l^+l^- + b + \not{E}_T)$	0.565 ± 0.005	1.4×10^{-4}
diboson $(\to l^+l^- + b\bar{b} + \not{E}_T)$	0.908 ± 0.001	1.1×10^{-3}
$Z + \text{jets}(\to l^+l^- + jets)$	287 ± 2	1.1×10^{-5}

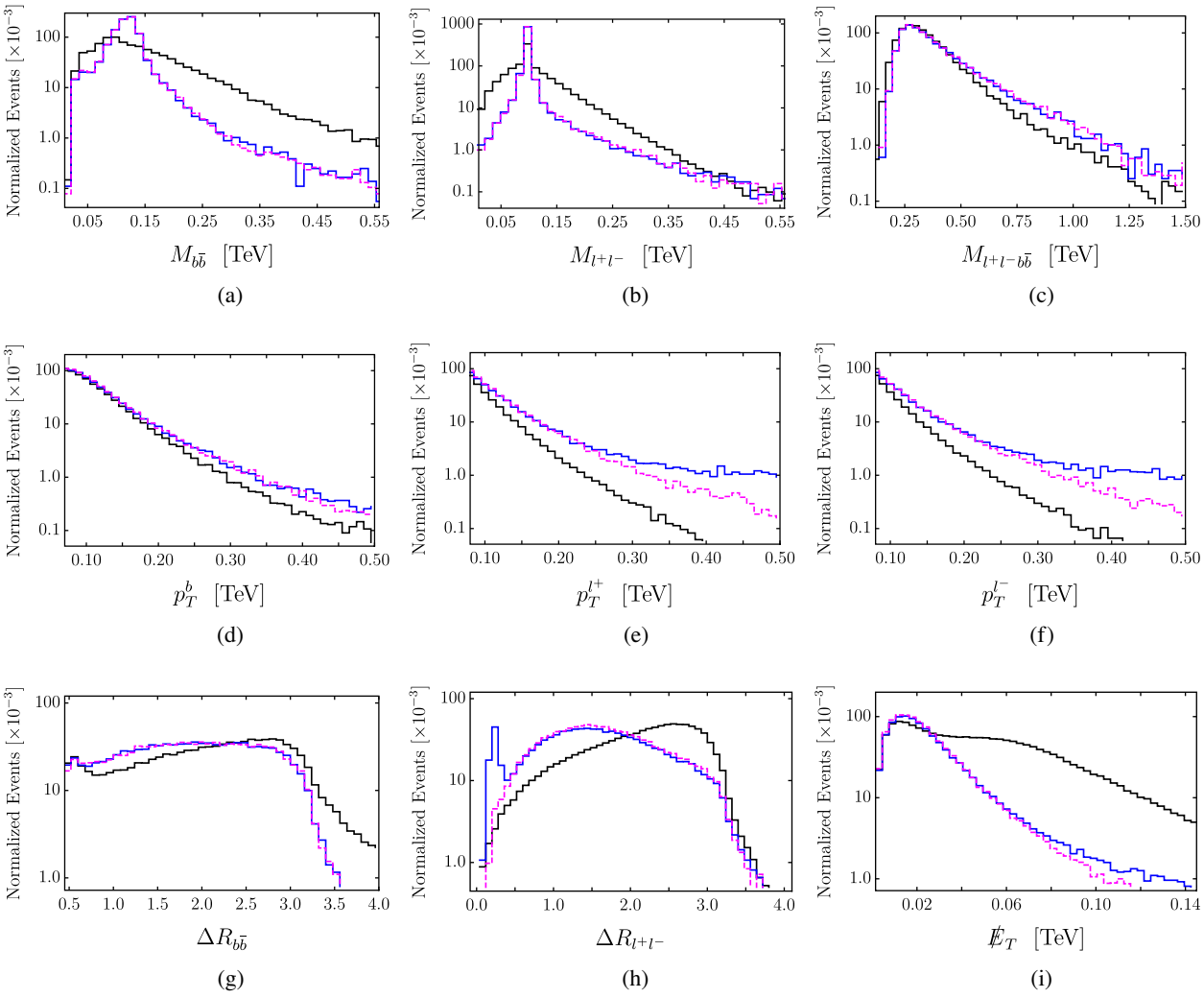

FIG. 5. Reconstructed level event distributions for the composite Higgs signal with $\Gamma_{1,2}/m_{1,2} = 1\%$ (blue), 20% (magenta, dashed), and the combined background events (black) are shown. The benchmark values of the model parameters are same as in Fig. 4.

the cleaner leptonic channel, which may be a better discriminator away from the pole. Our analysis emphasizes the importance of studying these differential distributions to probe a nonelementary nature of Higgs boson at the future runs of LHC.

IV. REACH AT HL-LHC

In this section, we discuss the reach of HL-LHC to explore the parameter space of the composite Higgs couplings to Z bosons in the associated Higgs production channel. The HL-LHC is expected to run at a center of mass energy of 14 TeV and collect data till 3 ab^{-1} of integrated luminosity with the provision to reach up to 4 ab^{-1} [44]. The major backgrounds at the LHC from the signal channel considered here come from the $t\bar{t}$, single top in the tW channel, diboson, and $Z+$jets events. We generate the background events by imposing the same generator level cuts given in the Table I. The LO cross sections and efficiencies for the signal and background processes are displayed in the Table II. In Fig. 5, we present the normalized kinematic distributions of various observables for both the background and the composite Higgs signals by generating 10^5 events in each case. Taking cue from the distributions presented in Fig. 5, we

TABLE III. Reconstructed level cuts used to focus on the tails of the distributions.

Observable	p_T^b	p_T^l	$M_{l^+l^-}$	$M_{b\bar{b}}$	$\Delta R_{l^+l^-,b\bar{b}}$	$M_{l^+l^-b\bar{b}}$	$\not{E}_{T,miss}$
Cut	> 50 GeV	> 50 GeV	> 80 GeV	> 80 GeV	< 2.0	> 500 GeV	< 70 GeV

devise the reconstructed level cuts as summarized in Table III. In the standard Higgs searches performed by CMS and ATLAS [73,74], cuts on $M_{l^+l^-}$ and $M_{b\bar{b}}$ are designed to focus on the Higgs peak, providing a huge discrimination between the signal and the backgrounds. On the other hand, we do not place any upper cut on the invariant momenta of the final states to focus on the tails of the distributions in order to maximize the deviation between the composite Higgs from the elementary Higgs scenario, at the cost of lowering overall signal to background significance. To account for the higher order (NLO) effects, we multiply the LO cross sections with the appropriate K factors for both the signal and the backgrounds, assuming that the efficiencies remain unchanged. In case of the composite Higgs signal, we have used the same K factor as obtained for the SM process which has been conservatively estimated as 1.2 [83]. The K factors for the background are 1.47 for $t\bar{t}$, 1.09 for singletop in the tW channel, 1.43 for diboson, and 1.35 for $Z+$ jets [75,84]. We generate composite Higgs signal events by varying both m_1 and m_2 from 1.5–3.5 TeV. The expected number of signal (S) and background (B) events at a certain integrated luminosity $\mathcal{L}$ is given by

$$S, B = \sigma_{S,B} \times \epsilon_{S,B} \times \mathcal{L}, \tag{4.1}$$

where $\sigma_{S,B}$ denote the signal and background cross sections obtained from MadGraph5 and multiplied with the appropriate K factors, respectively. The signal (background) efficiencies ϵ_S (ϵ_B), defined as the ratio of the number of signal (background) events surviving after applying the cuts listed in Table III to the initial number of events, are calculated for the elementary Higgs, the composite Higgs scenario, and the background processes by generating 5×10^4 (1.5×10^5 for backgrounds) events for each case. In Fig. 6, we present the contours of 5σ signal significance (defined as $S/\sqrt{B}$) in the $m_1 - m_2$ plane for 3 ab^{-1} (solid) and 4 ab^{-1} (dashed) integrated luminosities. In the same figure, the signal efficiency ϵ_S varies between [0.013–0.036] for $\Gamma_{1,2}/m_{1,2} = 1\%$ and [0.013–0.019] for $\Gamma_{1,2}/m_{1,2} = 20\%$, respectively. Using the cuts given in Table III, we find $S/\sqrt{B}$ for the elementary case are 3.92 and 4.53 at 3 ab^{-1} and 4 ab^{-1}, respectively. To show the percentage deviation between the composite Higgs signal from the elementary case, we define a quantity $\delta(m_1, m_2)$, as a function of $m_{1,2}$ as

$$\delta(m_1, m_2) \equiv 100 \times \frac{S_{\rm CH}(m_1, m_2) - S_{\rm EL}}{S_{\rm EL}}, \tag{4.2}$$

where we calculate the expected number of signal events $S_{\rm CH}(m_1, m_2)$ for the composite Higgs scenario and $S_{\rm EL}$ for the elementary case using the Eq. (4.1). The density plot in Fig. 6 shows the variation of $\delta(m_1, m_2)$ with the masses of the mesonic states. We find that the δ varies from 8%–30% (8%–20%) for $\Gamma_{1,2}/m_{1,2} = 1\%(20\%)$ in the region explorable with at least 5σ signal significance at 4ab^{-1} integrated luminosity and allowed by the conservative limit from the S parameter (shown by the black dashed line). Note that for both cases, the entire parameter space shown in the Fig. 6 has a signal significance more than 3σ. Inclusion of 1% background systematic uncertainty can reduce the significance by up to 30%. In Fig. 7, on the other hand, we show how the prospects of getting a 3σ (5σ) signal significance vary with the integrated luminosity for different values of $m_1 (= m_2)$. We observe that for $\Gamma_{1,2}/m_{1,2} = 1\%(20\%)$ and $\mathcal{L} \gtrsim 2.6$ ab^{-1} (3.3 ab^{-1}), a significant region of allowed parameter space can be probed with 5σ significance.

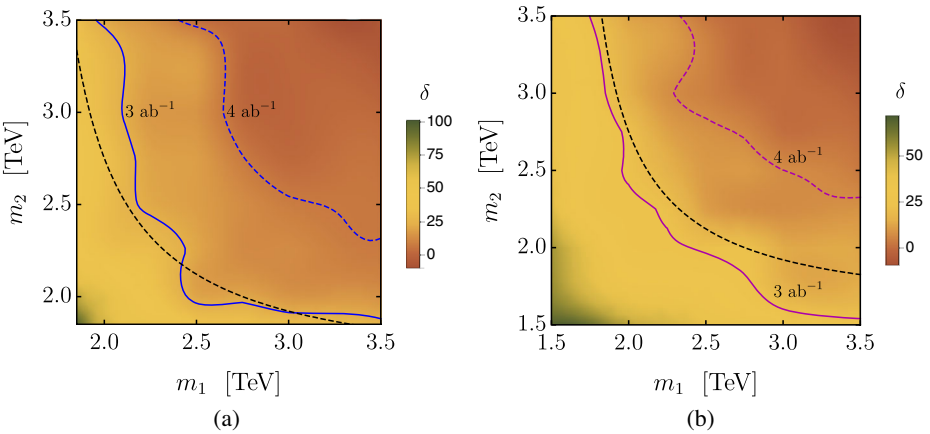

FIG. 6. Contours of 5σ signal significance in the $m_1 - m_2$ parameter space at 3 ab^{-1} (solid) and 4 ab^{-1} (dashed) integrated luminosity are shown for $\Gamma_{1,2}/m_{1,2} = 1\%$ (a) and 20% (b), respectively. The density plot shows the deviation of number of expected signal events in the composite Higgs scenario in comparison to the elementary case. The black dashed lines in both the panels denote the limits from the S-parameter at 99% CL [7].

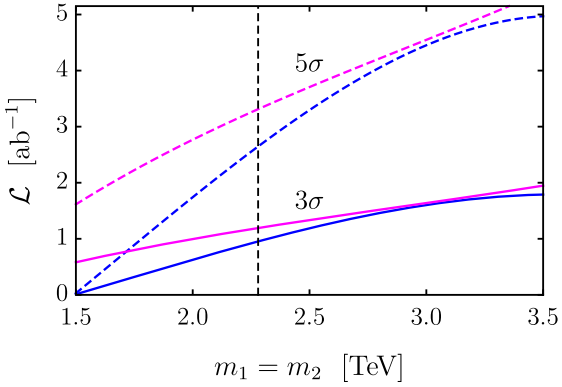

FIG. 7. 5σ (dashed) and 3σ (solid) contours in the $(m_1 = m_2) - \mathcal{L}$ plane for $\Gamma_{1,2}/m_{1,2} = 1\%$ (blue) and 20% (magenta). The black dashed line denotes the limit from the S parameter at 99% CL [7].

V. CONCLUSIONS

In this paper, we demonstrate that a possible geometric shape of the Higgs boson may be probed at the future runs of the LHC, even if the compositeness scale is just beyond accessible range, by investigating the differential distributions of various Higgs production and decay channels. As a proof of principle, we focus on the $pp \to Z^*H \to l^+l^-b\bar{b}$ channel in this paper.

The couplings of composite pNGB Higgs boson with other SM particles are written in terms of momentum dependent form factors, which capture the essential features of the underlying strong dynamics. We construct the form factor involved in the three-point hVV vertex from a bottom up approach, taking into account the results from large N formalism. The collider analysis for the $pp \to Z^*H \to l^+l^-b\bar{b}$ channel shows that even below the reach of the resonance scales, the composite Higgs signals start deviating from the elementary scenario, as is evident from Fig. 4. In this context, we observe that for the $pp \to Z^*H \to l^+l^-b\bar{b}$ channel, the distributions of the total invariant mass of the final states, their individual p_T and $\Delta R_{l^+l^-}$ may provide strong indications of a deviation from the elementary nature of the Higgs. It will be worthwhile to investigate the distributions of these (and other relevant) observables in more details at higher luminosity runs of the LHC. We further present the prospects for the HL-LHC to probe the Higgs form factor. Our conservative limits show that at 4 ab^{-1} integrated luminosity, 5σ signal significance can be achieved for a reasonable region of parameter space of the composite Higgs setup.

ACKNOWLEDGMENTS

We thank Gabriele Ferretti and Diogo Buarque Franzosi for useful discussions. A. B. acknowledges support from the Knut and Alice Wallenberg foundation (Grant No. KAW 2017.0100, SHIFT Project). A. B. was also supported by the Department of Atomic Energy, Government of India during the initial stage of the project. T. S. R. acknowledges Department of Science and Technology, Government of India, for support under Grant Agreement No. ECR/2018/002192 (Early Career Research Award). S. D. acknowledges MHRD, Government of India for the research fellowship.

APPENDIX: MAPPING TO THE SILH FRAMEWORK

To map the coefficients of the SILH Lagrangian with the form factor given in Eq. (2.9), we expand the latter up-to-leading order in $\mathcal{O}(p^2/m_\rho^2)$ as

$$\Pi_V^{\mu\nu} \simeq f^2\Bigg[\left(1 - \frac{\xi}{2} + \frac{p_1^2 + p_2^2}{m_1^2}\right)\eta^{\mu\nu} + \frac{1}{m_1^2}\{c_2^V(\eta^{\mu\nu}p_1.p_2 - p_2^\mu p_1^\nu) + c_3^V p_1^\mu p_2^\nu + c_4^V p_1^\mu p_1^\nu + c_5^V p_2^\mu p_2^\nu\}\Bigg], \tag{A1}$$

where we have assumed $m_1 = m_2 = m_\rho$. In Table IV, we present the explicit expressions for the coefficients in Eq. (2.10) for which the SILH Lagrangian can be mapped to $\Pi_W^{\mu\nu}$ and $\Pi_Z^{\mu\nu}$. In Fig. 3, we have employed values of the SILH coefficients using the Table IV to match with the benchmark parameters chosen for the form factor

TABLE IV. Comparison between the coefficients of the SILH Lagrangian and the form factors.

SILH	Our parametrization
c_H	1
$c_W + c_{HW}(\frac{m_\rho}{4\pi f})^2$	1
$\cos^2\theta_W[c_W + c_{HW}(\frac{m_\rho}{4\pi f})^2] + \sin^2\theta_W[c_B + c_{HB}(\frac{m_\rho}{4\pi f})^2]$	1
$2c_{HW}(\frac{m_\rho}{4\pi f})^2$	c_2^W
$2(\cos^2\theta_W c_{HW} + \sin^2\theta_W c_{HB})(\frac{m_\rho}{4\pi f})^2$	c_2^Z
0	$c_3^W = c_3^Z$
$c_W + c_{HW}(\frac{m_\rho}{4\pi f})^2$	$-c_4^W = -c_5^W$
$\cos^2\theta_W[c_W + c_{HW}(\frac{m_\rho}{4\pi f})^2] + \sin^2\theta_W[c_B + c_{HB}(\frac{m_\rho}{4\pi f})^2]$	$-c_4^Z = -c_5^Z$

TABLE V. Limits at 95% CL on the coefficients of the SILH Lagrangian. In the last column, we provide our choice of parameters with $f = 1$ TeV and $m_\rho = m_1 = m_2 = 2.5$ TeV.

Coefficients	Relation with c_i	Global fit [69]	ATLAS [70]	CMS [71]	Our choice
$\bar{c}_H$	$c_H \frac{v^2}{f^2}$	$[-2.3, 0.1]$	⋯	⋯	0.06
$\bar{c}_W + \bar{c}_B$	$(c_W + c_B)\frac{M_W^2}{m_\rho^2}$	$[-0.05, 0.05]$	0	0	0.001
$\bar{c}_W - \bar{c}_B$	$(c_W - c_B)\frac{M_W^2}{m_\rho^2}$	$[-0.12, 0.04]$	$[-0.006, 0.014]$	$[-0.09, 0.08]$	0
$\bar{c}_{HW}$	$c_{HW}\frac{M_W^2}{16\pi^2 f^2}$	$[-0.03, 0.03]$	$[-0.003, 0.008]$	$[-0.08, 0.08]$	0.0005
$\bar{c}_{HB}$	$c_{HB}\frac{M_W^2}{16\pi^2 f^2}$	$[-0.05, 0.02]$	$[-0.022, 0.049]$	⋯	0.0005

parametrization. In particular, we assume $c_H = 1$, $c_W = c_B = 1/2$, and $c_{HW} = c_{HB} = (8\pi^2 f^2/m_1^2) \simeq 12$. Note that the form factor approach strongly correlates with the SILH coefficients. Bounds on the SILH coefficients are generally given in terms of the dimensionless parameters $\bar{c}_i \equiv c_i(M_W^2/\Lambda^2)$ [69–72], where Λ denotes the new physics scale. In Table V, current limits on the SILH coefficients and our choice of benchmark values are summarized. From the table, it is evident that our choice of parameters is well within the present experimental bounds. We also list the explicit relations between $\bar{c}_i$ and the coefficients of each operators appearing in Eq. (2.10).

[1] G. Aad *et al.* (ATLAS Collaboration), Observation of a new particle in the search for the Standard Model Higgs boson with the ATLAS detector at the LHC, Phys. Lett. B **716**, 1 (2012).

[2] S. Chatrchyan *et al.* (CMS Collaboration), Observation of a new boson at a mass of 125 GeV with the CMS experiment at the LHC, Phys. Lett. B **716**, 30 (2012).

[3] D. B. Kaplan and H. Georgi, $SU(2) \times U(1)$ breaking by vacuum misalignment, Phys. Lett. **136B**, 183 (1984).

[4] M. J. Dugan, H. Georgi, and D. B. Kaplan, Anatomy of a composite Higgs model, Nucl. Phys. **B254**, 299 (1985).

[5] R. Contino, Y. Nomura, and A. Pomarol, Higgs as a holographic pseudoGoldstone boson, Nucl. Phys. **B671**, 148 (2003).

[6] K. Agashe, R. Contino, and A. Pomarol, The minimal composite Higgs model, Nucl. Phys. **B719**, 165 (2005).

[7] R. Contino, The Higgs as a composite Nambu-Goldstone boson, in Physics of the large and the small, TASI 09, Proceedings of the Theoretical Advanced Study Institute in Elementary Particle Physics, Boulder, Colorado, USA, 2009 (2011), pp. 235–306, https://doi.org/10.1142/9789814327183_0005.

[8] G. Panico and A. Wulzer, The composite Nambu-Goldstone Higgs, Lect. Notes Phys. **913**, 1 (2016).

[9] J. Erdmenger, N. Evans, W. Porod, and K. S. Rigatos, Gauge/Gravity Dynamics for Composite Higgs Models and the Top Mass, Phys. Rev. Lett. **126**, 071602 (2021).

[10] J. Erdmenger, N. Evans, W. Porod, and K. S. Rigatos, Gauge/gravity dual dynamics for the strongly coupled sector of composite Higgs models, J. High Energy Phys. 02 (2021) 058.

[11] J. Barnard, T. Gherghetta, and T. S. Ray, UV descriptions of composite Higgs models without elementary scalars, J. High Energy Phys. 02 (2014) 002.

[12] G. Ferretti and D. Karateev, Fermionic UV completions of composite Higgs models, J. High Energy Phys. 03 (2014) 077.

[13] G. Ferretti, UV completions of partial compositeness: The case for a SU(4) gauge group, J. High Energy Phys. 06 (2014) 142.

[14] R. Barcelo, A. Carmona, M. Chala, M. Masip, and J. Santiago, Single vectorlike quark production at the LHC, Nucl. Phys. **B857**, 172 (2012).

[15] A. De Simone, O. Matsedonskyi, R. Rattazzi, and A. Wulzer, A first top partner Hunter's guide, J. High Energy Phys. 04 (2013) 004.

[16] A. Azatov, D. Chowdhury, D. Ghosh, and T. S. Ray, Same sign di-lepton candles of the composite gluons, J. High Energy Phys. 08 (2015) 140.

[17] S. Moretti, D. O'Brien, L. Panizzi, and H. Prager, Production of extra quarks at the large hadron collider beyond the narrow width approximation, Phys. Rev. D **96**, 075035 (2017).

[18] G. Cacciapaglia, A. Carvalho, A. Deandrea, T. Flacke, B. Fuks, D. Majumder, L. Panizzi, and H.-S. Shao, Next-to-leading-order predictions for single vector-like quark production at the LHC, Phys. Lett. B **793**, 206 (2019).

[19] S. Dasgupta, S. K. Rai, and T. S. Ray, Impact of a colored vector resonance on the collider constraints for top-like top partner, Phys. Rev. D **102**, 115014 (2020).

[20] M. Low, A. Tesi, and L.-T. Wang, Composite spin-1 resonances at the LHC, Phys. Rev. D **92**, 085019 (2015).

[21] C. Niehoff, P. Stangl, and D. M. Straub, Direct and indirect signals of natural composite Higgs models, J. High Energy Phys. 01 (2016) 119.

[22] D. Buarque Franzosi, G. Cacciapaglia, H. Cai, A. Deandrea, and M. Frandsen, Vector and Axial-vector resonances in composite models of the Higgs boson, J. High Energy Phys. 11 (2016) 076.

[23] D. Liu, L.-T. Wang, and K.-P. Xie, Prospects of searching for composite resonances at the LHC and beyond, J. High Energy Phys. 01 (2019) 157.

[24] A. Falkowski, Pseudo-goldstone Higgs production via gluon fusion, Phys. Rev. D **77**, 055018 (2008).

[25] A. Banerjee, G. Bhattacharyya, N. Kumar, and T. S. Ray, Constraining composite Higgs models using LHC data, J. High Energy Phys. 03 (2018) 062.

[26] A. Banerjee and G. Bhattacharyya, Probing the Higgs boson through Yukawa force, Nucl. Phys. **B961**, 115261 (2020).

[27] E. Carragher, W. Handley, D. Murnane, P. Stangl, W. Su, M. White, and A. G. Williams, Convergent Bayesian global fits of 4D composite Higgs models, J. High Energy Phys. 05 (2021) 237.

[28] C. K. Khosa and V. Sanz, On the impact of the LHC Run2 data on general Composite Higgs scenarios, arXiv:2102.13429.

[29] Q.-H. Cao, L.-X. Xu, B. Yan, and S.-H. Zhu, Signature of pseudo Nambu–Goldstone Higgs boson in its decay, Phys. Lett. B **789**, 233 (2019).

[30] K.-P. Xie and B. Yan, Probing the electroweak symmetry breaking with Higgs production at the LHC, Phys. Lett. B **820**, 136515 (2021).

[31] B. Yan and C. P. Yuan, The Anomalous $Zb\bar{b}$ Couplings: From LEP to LHC, Phys. Rev. Lett. **127**, 051801 (2021).

[32] A. Azatov and A. Paul, Probing Higgs couplings with high p_T Higgs production, J. High Energy Phys. 01 (2014) 014.

[33] A. Azatov, C. Grojean, A. Paul, and E. Salvioni, Taming the off-shell Higgs boson, Zh. Eksp. Teor. Fiz. **147**, 410 (2015).

[34] H. Murayama, V. Rentala, and J. Shu, Probing strong electroweak symmetry breaking dynamics through quantum interferometry at the LHC, Phys. Rev. D **92**, 116002 (2015).

[35] B. Bellazzini, C. Csáki, J. Hubisz, S. J. Lee, J. Serra, and J. Terning, Quantum Critical Higgs, Phys. Rev. X **6**, 041050 (2016).

[36] A. Azatov, C. Grojean, A. Paul, and E. Salvioni, Resolving gluon fusion loops at current and future hadron colliders, J. High Energy Phys. 09 (2016) 123.

[37] D. Gonçalves, T. Han, and S. Mukhopadhyay, Higgs couplings at high scales, Phys. Rev. D **98**, 015023 (2018).

[38] D. Buarque Franzosi and A. Tonero, Top-quark partial compositeness beyond the effective field theory paradigm, J. High Energy Phys. 04 (2020) 040.

[39] D. Gonçalves, T. Han, S. Ching Iris Leung, and H. Qin, Off-shell Higgs couplings in $H^* \to ZZ \to \ell\ell\nu\nu$, Phys. Lett. B **817**, 136329 (2021).

[40] P. B. O. Souza, Phenomenology of theories with a compound Higgs, Master's Dissertation, Institute of Physics, University of São Paulo, São Paulo, 2020.

[41] G. 't Hooft, A planar diagram theory for strong interactions, Nucl. Phys. **B72**, 461 (1974).

[42] G. 't Hooft, A two-dimensional model for mesons, Nucl. Phys. **B75**, 461 (1974).

[43] E. Witten, Baryons in the $1/n$ expansion, Nucl. Phys. **B160**, 57 (1979).

[44] M. Cepeda *et al.*, Report from working group 2: Higgs physics at the HL-LHC and HE-LHC, CERN Yellow Rep. Monogr. **7**, 221 (2019).

[45] G. Isidori, A. V. Manohar, and M. Trott, Probing the nature of the Higgs-like Boson via $h \to V\mathcal{F}$ decays, Phys. Lett. B **728**, 131 (2014).

[46] G. Isidori and M. Trott, Higgs form factors in associated production, J. High Energy Phys. 02 (2014) 082.

[47] A. Pomarol and F. Riva, The composite Higgs and light resonance connection, J. High Energy Phys. 08 (2012) 135.

[48] D. Marzocca, M. Serone, and J. Shu, General composite Higgs models, J. High Energy Phys. 08 (2012) 013.

[49] A. Orgogozo and S. Rychkov, Exploring T and S parameters in vector meson dominance models of strong electroweak symmetry breaking, J. High Energy Phys. 03 (2012) 046.

[50] J. Galloway, A. L. Kagan, and A. Martin, A UV complete partially composite-pNGB Higgs, Phys. Rev. D **95**, 035038 (2017).

[51] A. Agugliaro, O. Antipin, D. Becciolini, S. De Curtis, and M. Redi, UV complete composite Higgs models, Phys. Rev. D **95**, 035019 (2017).

[52] T. Alanne, D. Buarque Franzosi, and M. T. Frandsen, A partially composite Goldstone Higgs, Phys. Rev. D **96**, 095012 (2017).

[53] G. F. Giudice, C. Grojean, A. Pomarol, and R. Rattazzi, The strongly-interacting light Higgs, J. High Energy Phys. 06 (2007) 045.

[54] A. Alloul, B. Fuks, and V. Sanz, Phenomenology of the Higgs effective lagrangian via FEYNRULES, J. High Energy Phys. 04 (2014) 110.

[55] F. Maltoni, K. Mawatari, and M. Zaro, Higgs characterisation via vector-boson fusion and associated production: NLO and parton-shower effects, Eur. Phys. J. C **74**, 2710 (2014).

[56] J. Ellis, V. Sanz, and T. You, Complete Higgs sector constraints on dimension-6 operators, J. High Energy Phys. 07 (2014) 036.

[57] A. Biekötter, A. Knochel, M. Krämer, D. Liu, and F. Riva, Vices and virtues of Higgs effective field theories at large energy, Phys. Rev. D **91**, 055029 (2015).

[58] K. Mimasu, V. Sanz, and C. Williams, Higher order QCD predictions for associated Higgs production with anomalous couplings to gauge bosons, J. High Energy Phys. 08 (2016) 039.

[59] J. Brehmer, A. Freitas, D. Lopez-Val, and T. Plehn, Pushing Higgs effective theory to its limits, Phys. Rev. D **93**, 075014 (2016).

[60] C. Degrande, B. Fuks, K. Mawatari, K. Mimasu, and V. Sanz, Electroweak Higgs boson production in the standard model effective field theory beyond leading order in QCD, Eur. Phys. J. C **77**, 262 (2017).

[61] C. Englert, R. Rosenfeld, M. Spannowsky, and A. Tonero, New physics and signal-background interference in associated $pp \to HZ$ production, Europhys. Lett. **114**, 31001 (2016).

[62] K. Agashe and R. Contino, The minimal composite Higgs model and electroweak precision tests, Nucl. Phys. **B742**, 59 (2006).

[63] A. Falkowski, F. Riva, and A. Urbano, Higgs at last, J. High Energy Phys. 11 (2013) 111.
[64] R. Contino and M. Salvarezza, One-loop effects from spin-1 resonances in Composite Higgs models, J. High Energy Phys. 07 (2015) 065.
[65] D. Ghosh, M. Salvarezza, and F. Senia, Extending the analysis of electroweak precision constraints in composite Higgs models, Nucl. Phys. **B914**, 346 (2017).
[66] M. Aaboud *et al.* (ATLAS Collaboration), Search for heavy resonances decaying into a W or Z boson and a Higgs boson in final states with leptons and b-jets in 36 fb^{-1} of $\sqrt{s} =$ 13 TeV pp collisions with the ATLAS detector, J. High Energy Phys. 03 (2018) 174.
[67] B. Bellazzini, C. Csaki, J. Hubisz, J. Serra, and J. Terning, Composite Higgs sketch, J. High Energy Phys. 11 (2012) 003.
[68] D. Buarque Franzosi and P. Ferrarese, Implications of vector boson scattering unitarity in composite Higgs models, Phys. Rev. D **96**, 055037 (2017).
[69] J. Ellis, C. W. Murphy, V. Sanz, and T. You, Updated global SMEFT Fit to Higgs, diboson and electroweak data, J. High Energy Phys. 06 (2018) 146.
[70] M. Aaboud *et al.* (ATLAS Collaboration), Measurement of VH, $\mathrm{H} \to \mathrm{b\bar{b}}$ production as a function of the vector-boson transverse momentum in 13 TeV pp collisions with the ATLAS detector, J. High Energy Phys. 05 (2019) 141.
[71] CMS Collaboration, Combined Higgs boson production and decay measurements with up to 137 fb^{-1} of proton-proton collision data at $\sqrt{s} = 13$ TeV, Technical Report No. CMS-PAS-HIG-19-005, CERN, Geneva, 2020.
[72] J. J. Ethier, G. Magni, F. Maltoni, L. Mantani, E. R. Nocera, J. Rojo *et al.*, Combined SMEFT interpretation of Higgs, diboson, and top quark data from the LHC, arXiv:2105.00006.
[73] A. M. Sirunyan *et al.* (CMS Collaboration), Observation of Higgs Boson Decay to Bottom Quarks, Phys. Rev. Lett. **121**, 121801 (2018).
[74] M. Aaboud *et al.* (ATLAS Collaboration), Observation of $H \to b\bar{b}$ decays and VH production with the ATLAS detector, Phys. Lett. B **786**, 59 (2018).
[75] J. Alwall, R. Frederix, S. Frixione, V. Hirschi, F. Maltoni, O. Mattelaer, H.-S. Shao, T. Stelzer, P. Torrielli, and M. Zaro, The automated computation of tree-level and next-to-leading order differential cross sections, and their matching to parton shower simulations, J. High Energy Phys. 07 (2014) 079.
[76] D. Liu, L.-T. Wang, and K.-P. Xie, Broad composite resonances and their signals at the LHC, Phys. Rev. D **100**, 075021 (2019).
[77] S. Jung, D. Lee, and K.-P. Xie, Beyond $M_{t\bar{t}}$: Learning to search for a broad $t\bar{t}$ resonance at the LHC, Eur. Phys. J. C **80**, 105 (2020).
[78] T. Sjöstrand, S. Ask, J. R. Christiansen, R. Corke, N. Desai, P. Ilten, S. Mrenna, S. Prestel, C. O. Rasmussen, and P. Z. Skands, An Introduction to PYTHIA 8.2, Comput. Phys. Commun. **191**, 159 (2015).
[79] M. Cacciari, G. P. Salam, and G. Soyez, FastJet user manual, Eur. Phys. J. C **72**, 1896 (2012).
[80] J. de Favereau, C. Delaere, P. Demin, A. Giammanco, V. Lemaître, A. Mertens, and M. Selvaggi (DELPHES 3 Collaboration), DELPHES3, A modular framework for fast simulation of a generic collider experiment, J. High Energy Phys. 02 (2014) 057.
[81] E. Conte, B. Fuks, and G. Serret, MadAnalysis 5, a user-friendly framework for collider phenomenology, Comput. Phys. Commun. **184**, 222 (2013).
[82] A. M. Sirunyan *et al.* (CMS Collaboration), Search for low mass vector resonances decaying into quark-antiquark pairs in proton-proton collisions at $\sqrt{s} = 13$ TeV, Phys. Rev. D **100**, 112007 (2019).
[83] J. Baglio, S. Dawson, S. Homiller, S. D. Lane, and I. M. Lewis, Validity of standard model EFT studies of VH and VV production at NLO, Phys. Rev. D **101**, 115004 (2020).
[84] D. Stolarski and A. Tonero, Constraining new physics with single top productionat LHC, J. High Energy Phys. 08 (2020) 036.